Numerical Analysis of the Localization of Pulmonary Nodules During Thoracoscopic Surgery by Ultra-wideband Radio Technology

Supplementary Information

Alberto Battistel [*1], Peter P. Pott[2], and Knut Möller[1]

[1]Institute of Technical Medicine (ITeM), Furtwangen University (HFU), Jakob-Kienzle-Strasse 17, 78054 Villingen-Schwenningen
[2]Institute of Medical Device Technology, University of Stuttgart, Pfaffenwaldring 9, 70569 Stuttgart Deutschland

Contents

[*]Alberto.Battistel@hs-furtwangen.de

1 Ring artifact and target depth

The ring artifact was given by the fact that the central antennas provided a stronger signal compared to the other antennas. The main reason for this was that this antenna was closer to the target than the other antennas especially when the target was in a shallow position as visible from Figure S1.1 which shows the antennas distances for the antenna positioned in central position (central), in lateral position either top-bottom or left-right (lateral), and in the angle position (angle). Clearly the difference in distances between the central antenna and the others is maximal at low depths.

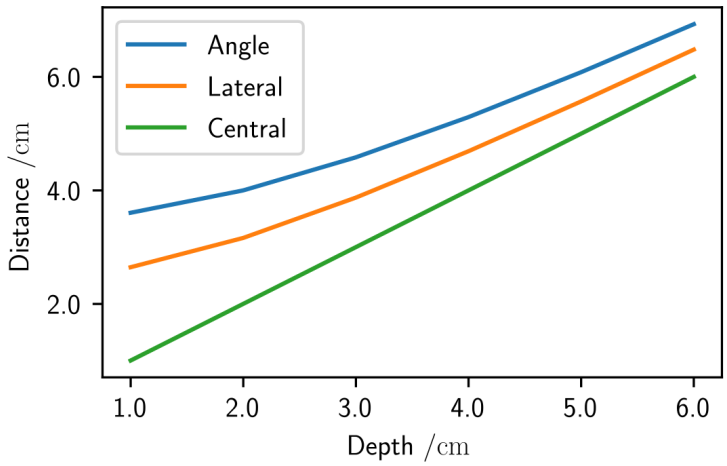

Figure S1.1: Antennas distances from the target at 1 GHz.

Figures S1.2 and S1.3 show the calibrated waveforms for the target depth of 1 cm and 6 cm, respectively for the simulation set at 1 GHz and 3×3 antenna distribution. As in the main article the waveforms are grouped according to their position in the antenna grid and this position is highlighted in gray at the top-right corner of every graph. Also the triangles, squares, and circles have the same meaning as in the main article. It can be seen that for the shallower target (Figure S1.2) the waveform intensity in (d) is much larger than in (a-c). On the other hand, in Figure S1.3 (a-d) the waveforms have comparable intensity. This supports the fact that ring artifact was an effect of the reciprocal distances between the antennas and the target.

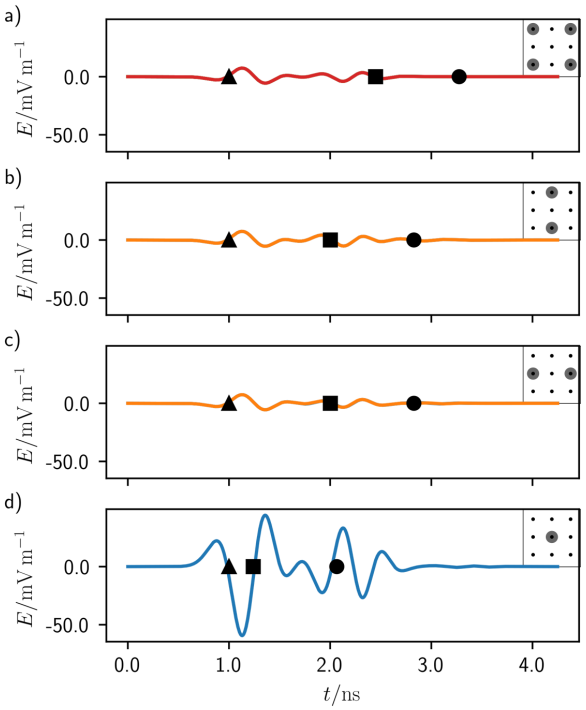

Figure S1.2: Calibrated waveforms B_n for a 1 cm deep target at 1 GHz central frequency and a 3×3 antenna grid. The black triangle, square, and circle represent, in order from left to right, the middle time of the pulse excitation and the return time for first and second interface of the target. a) Waveform for the angle antennas. b) Waveforms for the top and bottom central antennas. c) Waveforms for the left and right central antennas. d) Waveform for the central antenna.

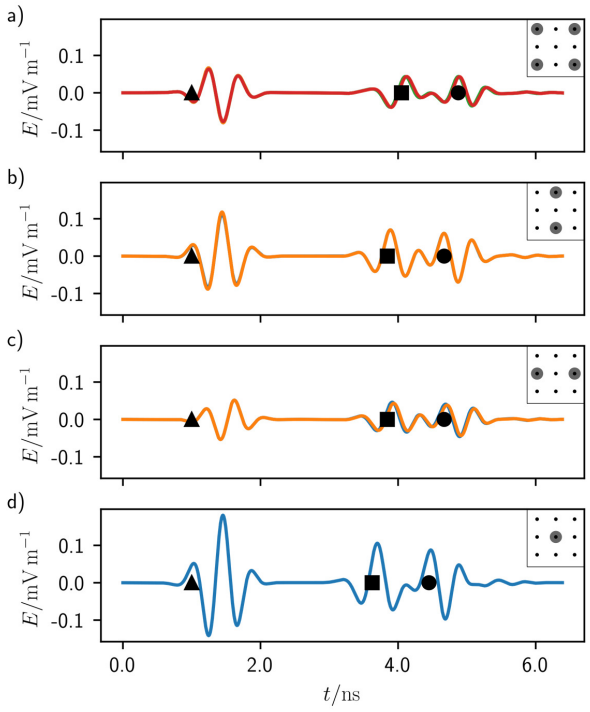

Figure S1.3: Calibrated waveforms B_n for a 6 cm deep target at 1 GHz central frequency and a 3×3 antenna grid. The black triangle, square, and circle represent, in order from left to right, the middle time of the pulse excitation and the return time for first and second interface of the target. a) Waveform for the angle antennas. b) Waveforms for the top and bottom central antennas. c) Waveforms for the left and right central antennas. d) Waveform for the central antenna.

2 Time separation between first and second echo

Figures S2.1 and S2.2 show the calibrated waveforms for the target depth of 3 cm and central frequency of 2 and 3 GHz, respectively and 3×3 antenna distribution. As expected, the time separation between the first echo (square) and the second one (circle) is smaller for Figure S2.2: 0.78 ns vs. 0.80 ns and it is 0.83 ns for Figure 4 in the main article. This confirms the fact that as the pulse frequency increases the second echo appears at larger and larger return times until it forms a completely separated pattern in the confocal images.

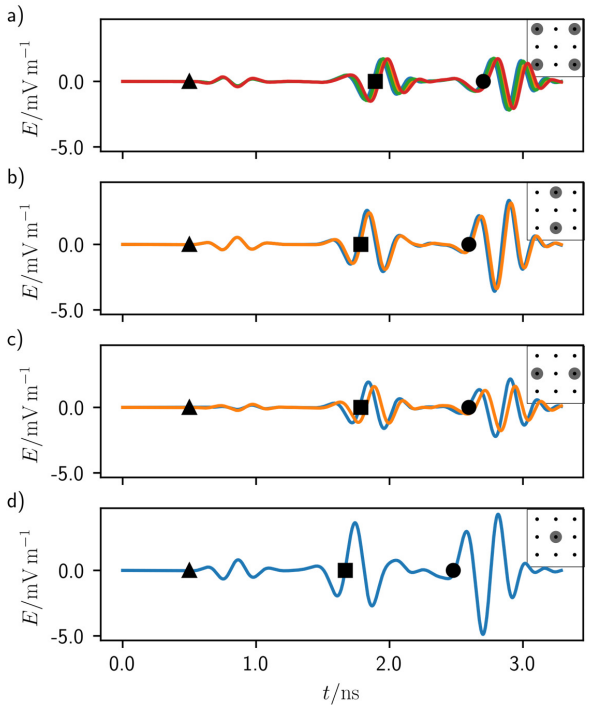

Figure S2.1: Calibrated waveforms B_n for a 3 cm deep target at 2 GHz central frequency and a 3×3 antenna grid. The black triangle, square, and circle represent, in order from left to right, the middle time of the pulse excitation and the return time for first and second interface of the target. a) Waveform for the angle antennas. b) Waveforms for the top and bottom central antennas. c) Waveforms for the left and right central antennas. d) Waveform for the central antenna.

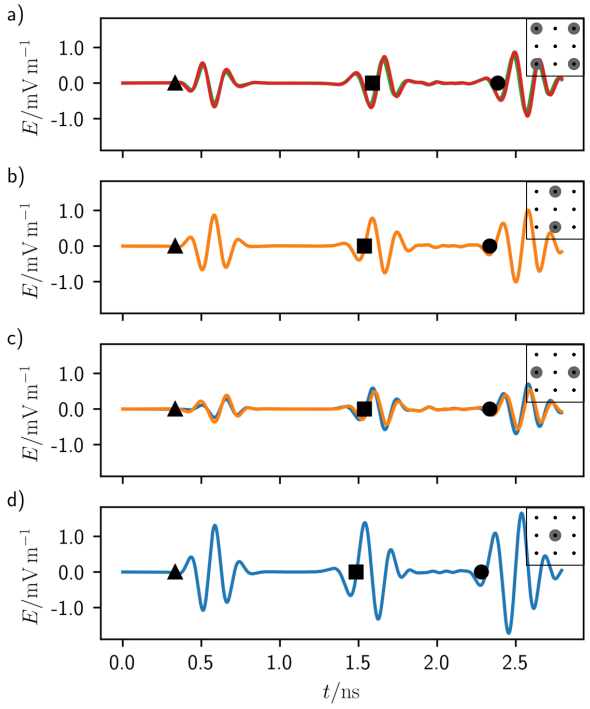

Figure S2.2: Calibrated waveforms B_n for a 3 cm deep target at 3 GHz central frequency and a 3×3 antenna grid. The black triangle, square, and circle represent, in order from left to right, the middle time of the pulse excitation and the return time for first and second interface of the target. a) Waveform for the angle antennas. b) Waveforms for the top and bottom central antennas. c) Waveforms for the left and right central antennas. d) Waveform for the central antenna.

3 Perfectly conductive target

Figures S3.1 shows the calibrated waveforms for a perfectly conductive target at the depth of 3 cm, 1 GHz of central frequency, and 3×3 antenna distribution. Comparing Figures S3.1 with Figure 4 of the main article it is clear that the second echo (circle) disappeared in the case of a perfectly conductive target. Since an electromagnetic wave cannot travel through a perfectly conductive material, this confirms that the second echo belongs to the backscattering of the electromagnetic wave from the bottom of the target when the electromagnetic wave travels through it. Also the intensity of the first echo was larger with a perfectly conductive target than with a nodule-realistic one. In fact a conductive object offers the maximal dielectric contrast.

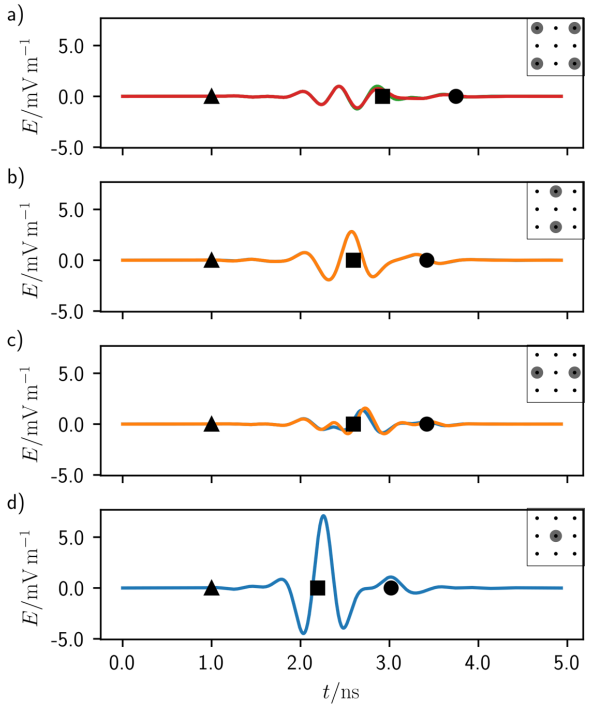

Figure S3.1: Calibrated waveforms B_n for a 3 cm deep perfectly conductive target at 1 GHz central frequency and a 3×3 antenna grid. The black triangle, square, and circle represent, in order from left to right, the middle time of the pulse excitation and the return time for first and second interface of the target. a) Waveform for the angle antennas. b) Waveforms for the top and bottom central antennas. c) Waveforms for the left and right central antennas. d) Waveform for the central antenna.

Figure S3.2 shows the confocal image for a 5×5 antenna distribution, 4 cm deep perfectly conductive target, and 1 GHz of central pulse frequency. Contrary to Figure 6 a) of the main article there is no appearance of a ghost target. Indeed given the elevated dielectric contrast, the target was well-localized. This confirms the fact that the ghost artifact was given by the echo at the bottom of the target.

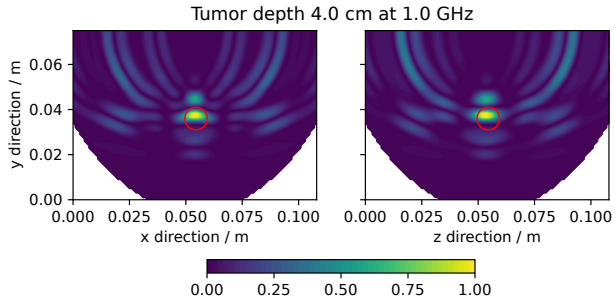

Figure S3.2: 5×5 confocal image of a perfectly conductive target at a depth of 4 cm and at a frequency of 2 GHz.

4 Time span of the echo modulation

Comparing Figures S4.1 with Figures S2.1 and S2.2 it is evident how the time span of the echos modulations change with the central frequency of the signal. In fact the span for the first echo (square) was circa 0.4, 0.6, and 0.8 ns for the Figure S2.1, S2.2, and S4.1, respectively which have 2, 3, and 4 GHz of central frequency. This supports the fact that at higher frequencies only the effective top part of the target can be localized.

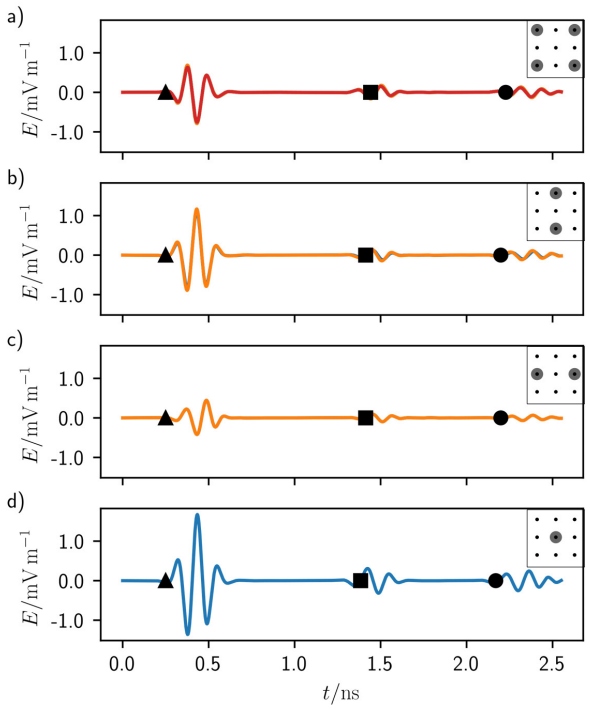

Figure S4.1: Calibrated waveforms B_n for a 3 cm deep target at 4 GHz central frequency and a 3×3 antenna grid. The black triangle, square, and circle represent, in order from left to right, the middle time of the pulse excitation and the return time for first and second interface of the target. a) Waveform for the angle antennas. b) Waveforms for the top and bottom central antennas. c) Waveforms for the left and right central antennas. d) Waveform for the central antenna.

5 Effect of the target size

Figure S5.1 and S5.2 show the comparison between the confocal images of two targets of different size at 6 cm of depth, with an antenna grid of 5×5, and at a frequency of 600 MHz. The targets have 2.5 mm and 5 mm of radius, respectively.

Although the pixel intensity of Figure S5.1 is lower than for Figure S5.2, the position of the target can still be identified. Consequently, the R ratio for Figure S5.1 was lower than for Figure S5.2: 23.3 against 26.3.

The wavelength of the electromagnetic wave in the lung tissue at 600 MHz is 6.7 cm. However, the target of smaller size could still be identified in the confocal map. This is a consequence of the fact that the target was in the antenna near-field, where the antenna has an higher sensitivity. It is also noteworthy that the ring artifacts were present in both confocal maps.

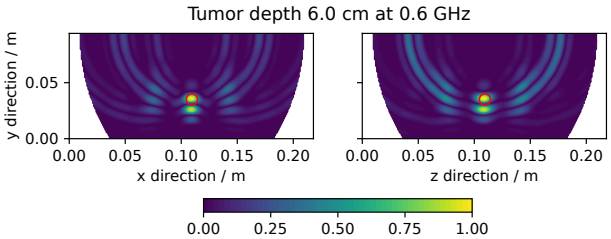

Figure S5.1: 5×5 confocal image of a target at a depth of 6 cm and at a frequency of 600 MHz.

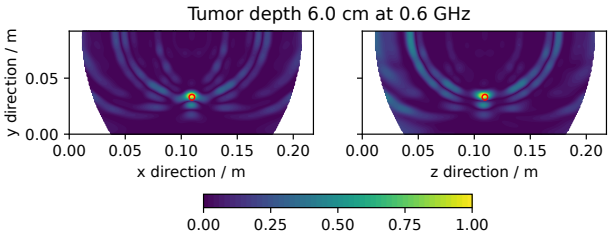

Figure S5.2: 5×5 confocal image of a target at a depth of 6 cm and at a frequency of 600 MHz.

6 Effect of the antenna model

Figure S6.1 and S6.2 show the confocal images made with the simplified antenna model and with a dipole, respectively. The dipole wire had an infinitesimal thickness, as it was made of the edges of cells through the gprMax command *#edge*, and a length of 4.2 cm which matched the wavelength in the lung tissue at the central frequency of the simulation, 1 GHz. Note that the confocal image made with the dipole has a larger size because of the sterical hindrance of the antenna. The target was at a depth of 3 cm.

It is noteworthy that the ring artifacts were present in both confocal maps, meaning that, although the simplified model used as antenna for the simulation cannot represent a physical antenna it can still give general guidelines.

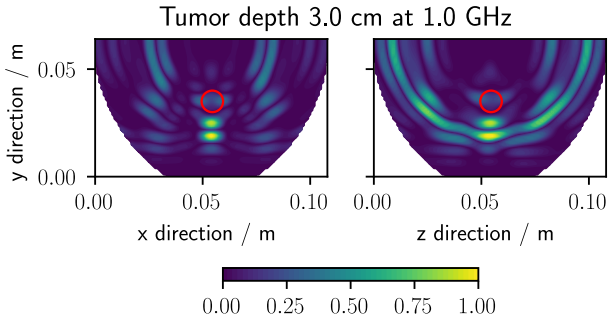

Figure S6.1: 3×3 confocal image of a target at a depth of 3 cm and at a frequency of 1 GHz with a simplified antenna model.

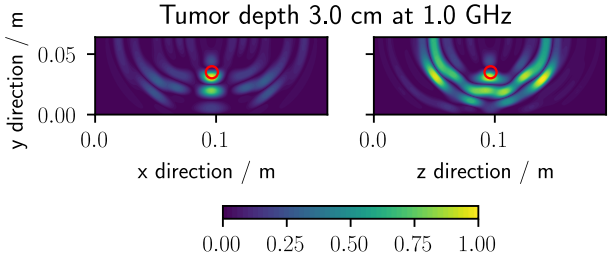

Figure S6.2: 3×3 confocal image of a target at a depth of 3 cm and at a frequency of 1 GHz with a dipole antenna.